

Reference-less algorithm for circumstellar disks imaging

Benoît Pairet^{1*}, Faustine Cantalloube², Laurent Jacques^{1*}

¹ISPGROUP, ICTEAM/ELEN, UCLouvain, Belgium ² Max Planck Institute for Astronomy, Germany

Abstract— Circumstellar disks play a key role in the understanding of stellar systems. Direct imaging of such extended structures is a challenging task. Current post-processing techniques, first tailored for exoplanets imaging, tend to produce deformed images of the circumstellar disks, hindering our capability to study their shape and photometry in details. We address here the reasons of this shortcoming and propose an algorithm that produces more faithful images of disks taken with ground-based telescopes. We also show that our algorithm is a good candidate for exoplanets imaging. We then explain how our approach can be extended in the form of a regularized inverse problem.

1 Introduction

Imaging stellar systems requires high contrast and high resolution to resolve the faint objects close to the much brighter hosting star. Ground based telescopes offer the highest resolution but suffer from atmospheric turbulence. Adaptive optics is used to correct the wavefront, thus allowing the use of a coronagraph which hides most of the starlight to unveil faint surrounding structures. Even with state-of-the-art hardware, there are remaining quasi-static aberrations forming speckles in the image, which prevent detection of faint signals. Specific observation methods are used to increase data diversity to disentangle the on-sky signals from the speckles. Angular differential imaging (ADI) is a popular observation method [5] where multiple snapshots of the star are taken through a night of observation in a way such that the speckles remain quasi-static while on-sky signals follow a deterministic circular trajectory, determined by the parallactic angles. Dedicated processing is then required to process ADI datasets. Among them, Principal components analysis (PCA) is a popular method [1, 11]. The reduction procedure, *i.e.*, the processing pipeline, goes as follows, (i) the $n \times n \times t$ spatiotemporal data cube is reshaped into a $\mathbb{R}^{T \times n^2}$ matrix \mathbf{Y} , (ii) we compute its low rank approximation, \mathbf{L} through an SVD, (iii) \mathbf{L} is subtracted from the data to form $\mathbf{S} = \mathbf{Y} - \mathbf{L}$ containing the on-sky signals, and (iv) the frames of \mathbf{S} are aligned to a common direction for the on-sky signal and temporally averaged to form the processed frame, we denote this last step as $\text{Red}(\mathbf{S})$. A detection is then usually performed either directly on the processed frame [6] or using the volume \mathbf{S} [9]. Throughout this paper, we write the best r rank approximation of a matrix \mathbf{X} as $\mathcal{H}_r^{\text{SVD}}(\mathbf{X})$.

Although ADI-based methods proved to be a powerful tool for exoplanets detection, observing circumstellar disks

remains an uneasy task as the shape of the disks is not known and can be quite irregular with smooth edges. The morphology of the disks is known to be severely impacted by the reduction procedure, hindering our capability to study the structure of the disks from ADI datasets. Very few attempts of tackling the problem of the disk deformation induced by the processing on ADI datasets have been made so far. We mention [7], in which the authors used a forward modeling of disks that they inject on the dataset to estimate the deformation induced by PCA. Another promising approach is found in [10] where the authors impose positivity on the processed frame by means of non-negative matrix factorization.

2 Our approach

In this short paper, we investigate the reasons behind the failure of PCA and provide an algorithm to overcome this shortcoming. First we illustrate the deformation induced by PCA on bright disks taken with the SPHERE high-contrast instrument [2] installed at the Very Large Telescope in Chile. The first is the ellipsoidal disk surrounding HR 4796A [8]. The second is the spiral disk surrounding SAO 206462 [4]. Fig. 1 shows the images of these disks obtained with PCA (top and middle, left). The disk around HR 4796A is supposed to have an ellipsoidal shape, but here we see negative (in dark) rotated copies of the disk on both sides of it. For SAO 206462, polarized images show its actual form (see [3]), we also see negative artifacts surrounding the signal of the disk which is distorted by the PCA process. The processing relies on the SVD where $\mathbf{Y} = \mathbf{U}\mathbf{\Sigma}\mathbf{V}^T$. In our setting, the matrix $\mathbf{V} \in \mathbb{R}^{T \times n^2}$ is a list of T $n \times n$ images (each images being reshaped into a vector in \mathbb{R}^{n^2} , by a slight abuse of notation, we call them images throughout this paper), $\mathbf{\Sigma}$ is a list of weight attributed to each image, and the time variation is encoded in \mathbf{U} where different weights are assigned to each image of \mathbf{V} through the temporal evolution.

By analyzing the images encoded in \mathbf{V} , we see that the way the disk is encoded in these images causes the deformation in the PCA processed frame. This is emphasized when building \mathbf{S} as the polar decomposition of \mathbf{Y} , *i.e.*, as $\mathbf{S} = \mathbf{U}\mathbf{V}^T$, where we see the same kind of deformations without any “self-absorption”.

Because the disk rotates, it has to be present in the images sequence at different positions. Unfortunately, the reference images \mathbf{V} do not encode the temporal evolution. Hence the disk must be represented in \mathbf{V} with positive and negative rotated copies whose linear combinations explain the temporal evolution of the disk. The left image of Fig. 2 shows the 6th image of \mathbf{V} , where we can see this effect clearly.

The proposed algorithm iteratively subtracts the best

*BP and LJ are funded by the Belgian F.R.S.-FNRS. Part of this study is funded by the project AlterSense (MIS-FNRS)

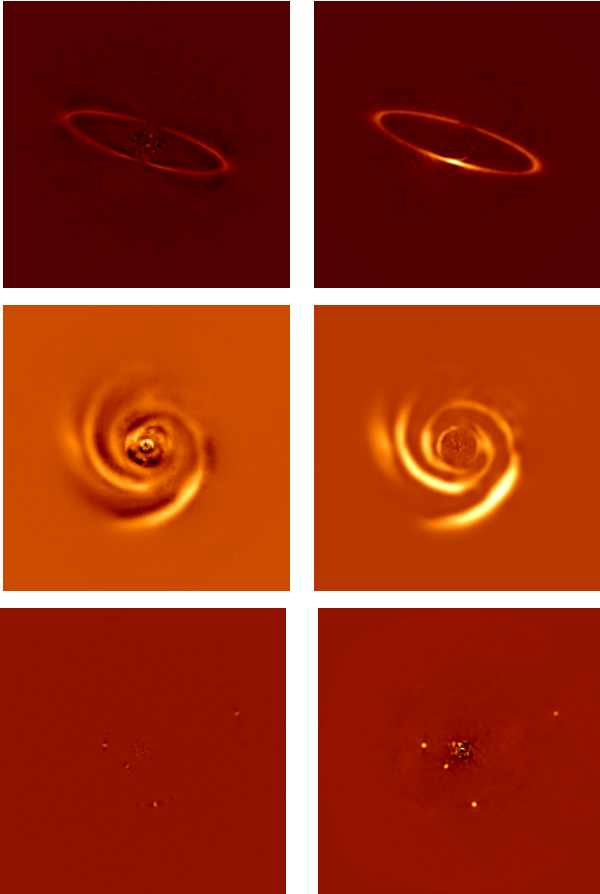


Figure 1: Processed frames using PCA (left) and our algorithm (right) for HR 4796A (top), SAO 206462 (middle), and HR 8799 (bottom). The colorbars are arbitrary but are consistent between left and right. Both disks are deformed in the PCA-processing. The shapes of the disks are closer to their actual shapes, obtained using polarimetric differential imaging. For HR 8799, the processed frame exhibits the typical PCA-induced deformation: two negative regions next to the planets. On the other hand, our algorithm yields a frame where planets have a round shape and we can even see the second ring of the Airy disk.

estimate of the disk from the data so its impact onto the images of \mathbf{V} decreases. To motivate this, we show that using an estimate from a PCA-processed frame significantly reduces the impact of the disk on \mathbf{V} . We compute the processed frame with $\mathbf{L} = \mathcal{H}_1^{\text{SVD}}(\mathbf{Y})$ and keep only the positive parts of it and denote it \mathbf{d} . We then inject it in a $t \times n \times n$ cube and rotate the frames according to the parallactic angles, we denote this operation by $\mathbf{D} = \Theta(\mathbf{d})$. Fig. 2 (right) displays an image of \mathbf{V} obtained by the SVD of $\mathbf{Y} - \mathbf{D}$. We can see that in this case the disk structure does not appear as clearly as on Fig. 2 (left).

Then the algorithm iterates with $r = 1, \dots, p$ and we compute $\mathbf{S}^{(r)} = \mathbf{Y} - \mathcal{H}_r^{\text{SVD}}(\mathbf{Y} - \Theta(\text{Red}(\mathbf{S}^{(r-1)})))$. This is motivated by the idea that if a better approximation of the disk is removed from \mathbf{Y} , its impact on \mathbf{V} further decreases. In return if the disk has a lower impact on \mathbf{V} , we expect to get a better approximation of the disk.

The rest of the algorithm follows the classical ADI reduction, $\mathbf{S}^{(p)}$ is aligned and collapsed to form the processed frame \mathbf{f} . The full algorithm is summarized in Alg. 1. Fig. 1 (top and middle, right) displays the results of this algorithm applied to the two datasets shown earlier. For SAO 206462, comparing with results displayed on Figure 1 of [3], one can see that the proposed algorithm produced a well-rendered shape.

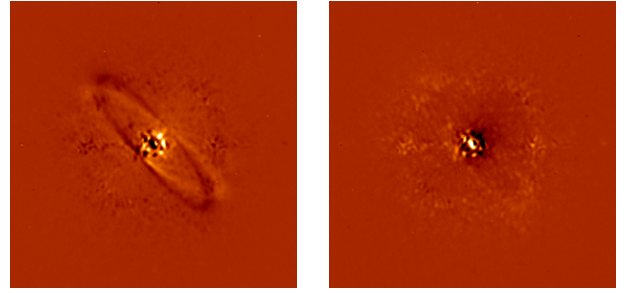


Figure 2: Difference in the morphology of the images of \mathbf{V} . Left, sixth image of \mathbf{V} built from \mathbf{Y} . Right, sixth image of \mathbf{V} built from $\mathbf{Y} - \mathbf{D}$. Where \mathbf{D} is the estimate of the disk. We can see that for the latter case, the intensity of the disk is significantly lower.

To further demonstrate the capability of our algorithm to preserve shapes, we applied it to exoplanets imaging, on the SPHERE data of HR 8799. For exoplanets, we know that the shape of the planets is similar to an Airy disk. We display the PCA-processed frame on Fig. 1 (bottom left). We observe the typical PCA-induced shape, the planet is surrounded by two negative regions. The results of our approach is displayed on Fig. 1 (bottom right). By a careful inspection, we can see that the Airy-disk like shape is rendered by our method, hence indicating that it is indeed shape preserving.

3 Conclusion

Alg. 1 shows promising results for both disks and exoplanets imaging. This algorithm is similar to a greedy version of a regularized inverse problem. It would then probably benefit from being formulated as a convex optimization program and solved exactly. To do so, we need to impose a low rank structure for \mathbf{L} , using the nuclear norm and “rotating 1-rank” structure for \mathbf{S} . This could be done using the Radon domain where an image rotation corresponds to a shift. This way, the temporal evolution of \mathbf{S} , *i.e.*, the rotation of the same frame, is encoded as a convolution with circular boundary conditions. We observed that the Radon transform preserves the low rank structure of \mathbf{L} . Hence the algorithm could be fully described in the Radon domain. This more rigorous approach is left as a future work.

We also showed that Alg. 1 can be used for exoplanets detection. In the processed frame the shape of the exoplanets is recovered. This provides the opportunity to further disentangle the exoplanet signal from residual noise by means of a deconvolution. This is left as future work.

Acknowledgements: The authors thank Julien Milli and Anne-Lise Maire for kindly providing the SPHERE datasets used in this study.

Algorithm 1

- 1: **Input:** \mathbf{Y}, m, p
 - 2: **Output:** \mathbf{f}
 - 3: $\mathbf{S}^{(0)} = \mathbf{Y} - \mathcal{H}_1^{\text{SVD}}(\mathbf{Y})$
 - 4: **for** $r = 1, 2, \dots, p$ **do**
 - 5: $\mathbf{S}^{(r)} = \mathbf{Y} - \mathcal{H}_r^{\text{SVD}}(\mathbf{Y} - \Theta(\text{Red}(\mathbf{S}^{(r-1)})))$
 - 6: **end for**
 - 7: $\mathbf{f} = \text{Red}(\mathbf{S}^{(p)})$
-

References

- [1] Adam Amara and Sascha P Quanz. Pynpoint: an image processing package for finding exoplanets. *Monthly Notices of the Royal Astronomical Society*, 427(2):948–955, 2012.
- [2] Jean-Luc Beuzit, Markus Feldt, Kjetil Dohlen, David Mouillet, Pascal Puget, Francois Wildi, Lyu Abe, Jacopo Antichi, Andrea Baruffolo, Pierre Baudoz, et al. Sphere: a planet finder instrument for the vlt. In *Ground-based and airborne instrumentation for astronomy II*, volume 7014, page 701418. International Society for Optics and Photonics, 2008.
- [3] Antonio Garufi, Sascha P Quanz, Henning Avenhaus, Esther Buenzli, Carsten Dominik, Farzana Meru, Michael R Meyer, Paola Pinilla, Hans Martin Schmid, and Sebastian Wolf. Small vs. large dust grains in transitional disks: do different cavity sizes indicate a planet?-sao 206462 (hd 135344b) in polarized light with vlt/naco. *Astronomy & Astrophysics*, 560:A105, 2013.
- [4] A-L Maire, Tomas Stolker, Sergio Messina, André Müller, Beth A Biller, Thayne Currie, Carsten Dominik, Carol A Grady, Anthony Boccaletti, Mickaël Bonnefoy, et al. Testing giant planet formation in the transitional disk of sao 206462 using deep vlt/sphere imaging. *Astronomy & Astrophysics*, 601:A134, 2017.
- [5] Christian Marois, David Lafreniere, René Doyon, Bruce Macintosh, and Daniel Nadeau. Angular differential imaging: A powerful high-contrast imaging technique. *The Astrophysical Journal*, 641(1):556, 2006.
- [6] Dimitri Mawet, Julien Milli, Zahed Wahhaj, Didier Pelat, Olivier Absil, Christian Delacroix, Anthony Boccaletti, Markus Kasper, Matthew Kenworthy, Christian Marois, et al. Fundamental limitations of high contrast imaging set by small sample statistics. *The Astrophysical Journal*, 792(2):97, 2014.
- [7] J Milli, D Mouillet, A-M Lagrange, A Boccaletti, D Mawet, G Chauvin, and M Bonnefoy. Impact of angular differential imaging on circumstellar disk images. *Astronomy & Astrophysics*, 545:A111, 2012.
- [8] Julien Milli, Arthur Vigan, David Mouillet, A-M Lagrange, J-C Augereau, Christophe Pinte, Dimitri Mawet, Hans Martin Schmid, Anthony Boccaletti, Luca Matrà, et al. Near-infrared scattered light properties of the hr 4796 a dust ring-a measured scattering phase function from 13.6 to 166.6. *Astronomy & Astrophysics*, 599:A108, 2017.
- [9] Benoît Pairet, Faustine Cantalloube, Carlos A. Gomez Gonzalez, Olivier Absil, and Laurent Jacques. Stim map: detection map for exoplanets imaging beyond asymptotic gaussian residual speckle noise. *Submitted in Monthly Notices of the Royal Astronomical Society*, *arXiv preprint: arXiv:1810.06895*, 2018.
- [10] Bin Ren, Laurent Pueyo, Guangtun Ben Zhu, John Debes, and Gaspard Duchêne. Non-negative matrix factorization: Robust extraction of extended structures. *The Astrophysical Journal*, 852(2):104, 2018.
- [11] Rémi Soummer, Laurent Pueyo, and James Larkin. Detection and characterization of exoplanets and disks using projections on karhunen-loève eigenimages. *The Astrophysical Journal Letters*, 755(2):L28, 2012.